

PAPER

Effect of topological patterning on self-rolling of nanomembranes

To cite this article: Cheng Chen *et al* 2018 *Nanotechnology* **29** 345301

View the [article online](#) for updates and enhancements.

You may also like

- [Strain-modulated photoelectric properties of self-rolled GaAs/Al_{0.26}Ga_{0.74}As quantum well nanomembrane](#)
Fei Zhang, XiaoFei Nie, GaoShan Huang et al.
- [Strain induced lifting of the charged exciton degeneracy in monolayer MoS₂ on a GaAs nanomembrane](#)
Jakub Jasiski, Akshay Balgarkashi, Valerio Piazza et al.
- [Strain-tuning of the optical properties of semiconductor nanomaterials by integration onto piezoelectric actuators](#)
Javier Martín-Sánchez, Rinaldo Trotta, Antonio Mariscal et al.





The Electrochemical Society

Advancing solid state & electrochemical science & technology

DISCOVER
how sustainability
intersects with
electrochemistry & solid
state science research



Effect of topological patterning on self-rolling of nanomembranes

Cheng Chen¹ , Pengfei Song^{2,3}, Fanchao Meng¹, Pengfei Ou¹, Xinyu Liu³  and Jun Song¹

¹ Department of Materials Engineering, McGill University, Montréal, Québec H3A0C5, Canada

² Department of Mechanical Engineering, McGill University, Montréal, Québec H3A0C3, Canada

³ Department of Mechanical and Industrial Engineering, University of Toronto, Toronto, Ontario M5S3G8, Canada

E-mail: jun.song2@mcgill.ca

Received 6 April 2018, revised 22 May 2018

Accepted for publication 31 May 2018

Published 14 June 2018



CrossMark

Abstract

The effects of topological patterning (i.e., grating and rectangular patterns) on the self-rolling behaviors of heteroepitaxial strained nanomembranes have been systematically studied. An analytical modeling framework, validated through finite-element simulations, has been formulated to predict the resultant curvature of the patterned nanomembrane as the pattern thickness and density vary. The effectiveness of the grating pattern in regulating the rolling direction of the nanomembrane has been demonstrated and quantitatively assessed. Further to the rolling of nanomembranes, a route to achieve predictive design of helical structures has been proposed and showcased. The present study provides new knowledge and mechanistic guidance towards predictive control and tuning of roll-up nanostructures via topological patterning.

Supplementary material for this article is available [online](#)

Keywords: roll-up, topological patterning, strained nanomembranes, helical structures, anisotropic

(Some figures may appear in colour only in the online journal)

1. Introduction

With continuous progression towards device and component miniaturization in nanotechnology, there is increasing demand in design flexibility and geometry variability [1–3]. Self-rolling of nanomembranes, where a strained bilayer (or multilayer) thin film scrolls up to form a three-dimensional (3D) structure, provides a powerful fabrication route towards realizing various 3D nanoscale configurations, such as nanotubes [4, 5], helix [6], and wrinkles [7, 8]. These unique 3D structures, combined with a plentiful pool of available functional materials, has motivated numerous applications in nanotechnology, such as microscale resonators [9–11], smart energy storage devices [12–14], and micro engines [15, 16], where the roll-up nanostructures are employed as primary architecture units, promoting great technological progress in micro/nano-electro-mechanical systems and lab on a chip [17–20].

However, the fabrication and obtainment of those sophisticated non-planar roll-up nanostructures are heavily dependent on the topographic patterning technique that pre-define the initial planar geometry to guide the deposition or removal of material of the strain engineered nanomembrane in order to achieve a higher level of manipulation over the rolling process [21–24]. For instance, the patterned grating structures have proved to be an effective strategy that can define and control the rolling direction of strained nanomembranes to facilitate the fabrication of complex structure of micro-/nano-springs [25]. The patterned U-shape nanomembranes are necessary in microtube optical sensors for lifting-up the middle part of the microtube from the substrate after rolling-up [9, 26]. Meanwhile, the topographic patterning also plays an important role in the integration of state-of-the-art functionality with well-designed optical or electrical modules, providing exceptional design and fabrication

flexibilities into targeted devices, thus enhancing the performance of existing structures and devices [27, 28].

The accurate design and fabrication of sophisticated roll-up configurations with patterns necessitate in-depth understanding of the mechanics underlying the rolling-up. Many analytical and numerical methods [29–34] have been developed, attempting to quantitatively simulate the roll-up process and to determine the resultant roll-up curvature [35–43]. However, in those previous modeling efforts, the effects of local thickness variation and nonuniform distribution of mismatch strain induced by patterning have not been considered.

The present study aims to address the afore-mentioned deficit in the modeling and simulation of self-rolling of patterned nanomembranes. Based on Von-Karman shell theory [44, 45] and Ritz method [46, 47], a comprehensive analytical model has been formulated. The new model quantitatively accounts for the effect of topographic patterning on the rolling direction and curvature of rolled-up nanomembranes. The accuracy and reliability of the analytical prediction from our model have been confirmed by finite-element (FE) simulations. Furthermore, the implication of our results to the design of more complex 3D roll-up structures (e.g., helical structures) was discussed, and a strategy to design helixes of well controlled geometric metrics, from a patterned host nanomembrane was demonstrated.

2. Methodology

2.1. Analytical formulation

Figure 1 illustrates the rectangular nanomembrane model considered in the present study. The length and width of the nanomembrane are denoted as L and W , with two axes, x_1 and x_2 , indicating the length and width directions respectively, also referred to as longitude (x_1) and lateral (x_2) directions below. The nanomembrane system comprises of two principle material layers, a passive substrate and an active film, denoted below as top and bottom layers respectively. On top of these two layers resides an additional pattern layer that may vary in size, density and thickness. The top layer with Young's modulus E_t , Poisson's ratio ν_t , and thicknesses h_t , is subject to initial mismatch strain ε_0 that originates from lattice mismatch or thermal loading. The elastic properties of the bottom layer of thickness h_b are characterized by Young's modulus E_b and Poisson's ratio ν_b . Without loss of generality, the patterned material is assumed to be the same as the top layer with thickness h_p . In particular, the patterns can be divided into two categories, i.e., attached and etched patterns. These two categories can be self-consistently characterized as $h_p > 0$ (attached) and $h_p < 0$ (etched). Here for ease of modeling we also define a dimensionless thickness parameter, $H_p = h_p/h_t$, to reflect the pattern induced relative thickness change for the top layer. Regarding the pattern layer, here we consider two typical patterns, i.e., grating and rectangular patterns, and for each case, we assume the pattern to be uniform in size, density and thickness, and that the width of the grating pattern or length/width of the cubic pattern are much smaller than the

resultant roll-up radius of curvature, for simplicity. Aiming at quantitatively evaluating the size effect of patterns, two parameters (ρ_1, ρ_2) are used to indicate the area density of the pattern layer. The density parameters ρ_1 and ρ_2 are defined as the ratios between the patterned area and normal area within the pattern-containing unit strips along x_1 and x_2 directions respectively (see figure 1(c)). It is apparent that when both ρ_1 and ρ_2 are finite (see figure 1(d)), the cubic patterns are achieved, otherwise we obtain the grating patterns (see figures 1(e), (f)).

In our calculations, the relations of strain ε and displacement field \mathbf{u} in a deformed nanomembrane in a given coordinate (x_1, x_2, x_3) (see figure 1(a)) are determined based on the Von-Karman nonlinear theory [48, 49] describing the large transverse deflections of thin shell, as shown below,

$$\varepsilon_{\alpha\beta} = \frac{1}{2} \left(\frac{\partial u_\alpha}{\partial x_\beta} + \frac{\partial u_\beta}{\partial x_\alpha} + \frac{\partial u_3}{\partial x_\beta} \cdot \frac{\partial u_3}{\partial x_\alpha} \right) - x_3 \frac{\partial^2 u_3}{\partial x_\alpha \partial x_\beta}, \quad (1)$$

with the stress σ is related to strain through Young's modulus E and Poisson's ratio ν in the following compact form:

$$\sigma_{\alpha\beta} = \frac{E}{(1+\nu)} \left(\varepsilon_{\alpha\beta} + \frac{\nu}{(1-\nu)} \varepsilon_{\gamma\gamma} \delta_{\alpha\beta} \right) - \frac{E\varepsilon_0}{(1-\nu)} \delta_{\alpha\beta}, \quad (2)$$

where the Greek subscripts α, β and $\gamma = 1, 2$, and ε_0 denotes the isotropic inelastic mismatch strain.

The displacement field \mathbf{u} , and subsequently the stress and strain fields can be obtained by minimizing the total strain energy $U = \int \int \int_V \frac{1}{2} \sigma_{ij} \varepsilon_{ij} dV$, where V represents the total volume of the strained nanomembrane. The existence of patterns, however, renders the surface nonuniform, in which case the strain energy can be divided into two parts:

$$U = U_n + U_p \quad (3)$$

with

$$U_n = \frac{1}{2} \int_0^{h_t+h_b} dx_3 \iint_{\Omega_{S_n}} (\sigma_{ij}^b \varepsilon_{ij}^b + \sigma_{ij}^t \varepsilon_{ij}^t) d\Omega_{S_n}, \quad (4)$$

$$U_p = \frac{1}{2} \int_0^{h_b+h_t+h_p} dx_3 \iint_{\Omega_{S_p}} (\sigma_{ij}^b \varepsilon_{ij}^b + \sigma_{ij}^t \varepsilon_{ij}^t + \sigma_{ij}^p \varepsilon_{ij}^p) d\Omega_{S_p}, \quad (5)$$

where U_n and U_p represent the strain energies associated with the normal (pattern-free) area Ω_{S_n} and patterned area Ω_{S_p} respectively. The superscripts b, t and p in the stress and strain terms indicate their association with bottom, top and pattern layers respectively. Subsequently the equilibrium configurations of nanomembranes with specific patterns could be obtained via minimization of U based on the trial in-plane and out-of-plane displacement shape functions. An approximated displacement field, i.e., u_i ($i = 1, 2, 3$) of the mid-plane of the nanomembrane can be assumed to be [45–48]:

$$u_1(x_1, x_2) = \sum_{i=0}^3 \sum_{j=0}^3 A_{ij} x_1^i x_2^j, \quad (6)$$

$$u_2(x_1, x_2) = \sum_{i=0}^3 \sum_{j=0}^3 B_{ij} x_1^i x_2^j, \quad (7)$$

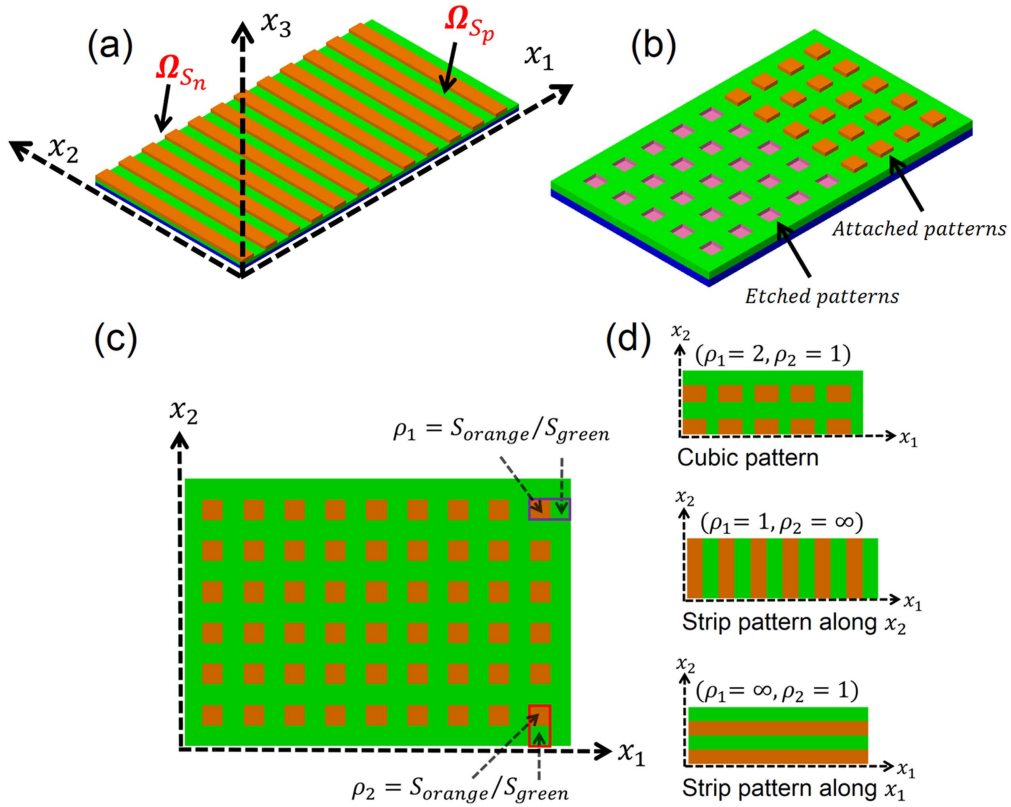


Figure 1. Schematic illustration of different pattern structures examined for the bilayer nanomembranes: (a) grating patterns colored in orange, (b) attached and etched cubic patterns, colored in orange and pink respectively. (c) Definition of the two pattern density parameters, ρ_1 and ρ_2 , with three representative examples of different pattern types/densities provided, as shown in (d).

Table 1. The relevant material properties of the two nanomembrane systems, $\text{GaAs}^{(\text{top})}/\text{In}_{0.2}\text{Ga}_{0.8}\text{As}^{(\text{bottom})}$ and $\text{GaN}^{(\text{top})}/\text{AlN}^{(\text{bottom})}$ [22, 53, 58] considered in the present study.

Material	Young's modulus E (GPa)	Poisson's ratio (ν)	Thicknesses (h_t or h_b) (nm)	Mismatch strain (ε_0)
GaAs	85.6	0.3	5.2	1.43%
$\text{In}_{0.2}\text{Ga}_{0.8}\text{As}$	75.1	0.3	5.8	
GaN	252	0.26	10	2.41%
AlN	297	0.3	10	

$$u_3 = \frac{1}{2}(ax_1^2 + bx_2^2), \quad (8)$$

where A_{ij} , B_{ij} , a , and b are adjustable parameters to be determined through the minimization of U . The above three-order polynomial approximation of the in-plane displacement field was proved to be sufficient to provide an accurate description for analyzing the deformation behaviors of thin film and shell structures [50, 51]. The curvature fields of the deformed nanomembrane can then be determined as:

$$\kappa_{11} = \frac{\partial^2 u_3}{\partial x_1^2} \text{ and } \kappa_{22} = \frac{\partial^2 u_3}{\partial x_2^2}. \quad (9)$$

2.2. Numerical simulations

FE simulations were employed for direct numerical simulations of the self-rolling behaviors of nanomembranes and validation of the analytical prediction of the resultant roll-up curvatures.

In this study, FE simulations were performed using the ABAQUS Unified FE software [52]. The layered structures with pre-defined patterns were created in the module of composite layups, and 4-node doubly curved thin/thick shell elements with reduced integration (S4R) were used to discretize the domain. The initial mismatch strain was achieved by assigning different thermal expansion coefficients to different layers and varying the temperature. Two categories of FE simulations were performed to examine the self-rolling behaviors of patterned nanomembranes, detailed as the follows:

- (1) *Category I:* for FE simulations in this category, the rolling process was examined using the static analysis process with large rotation considered. The direction of rolling is pre-defined with a moving boundary condition set up to achieve controlled release of the nanomembrane, where the model geometry is partitioned into ribbon segments (perpendicular to the rolling direction) and fixed initially, and then released gradually [53].

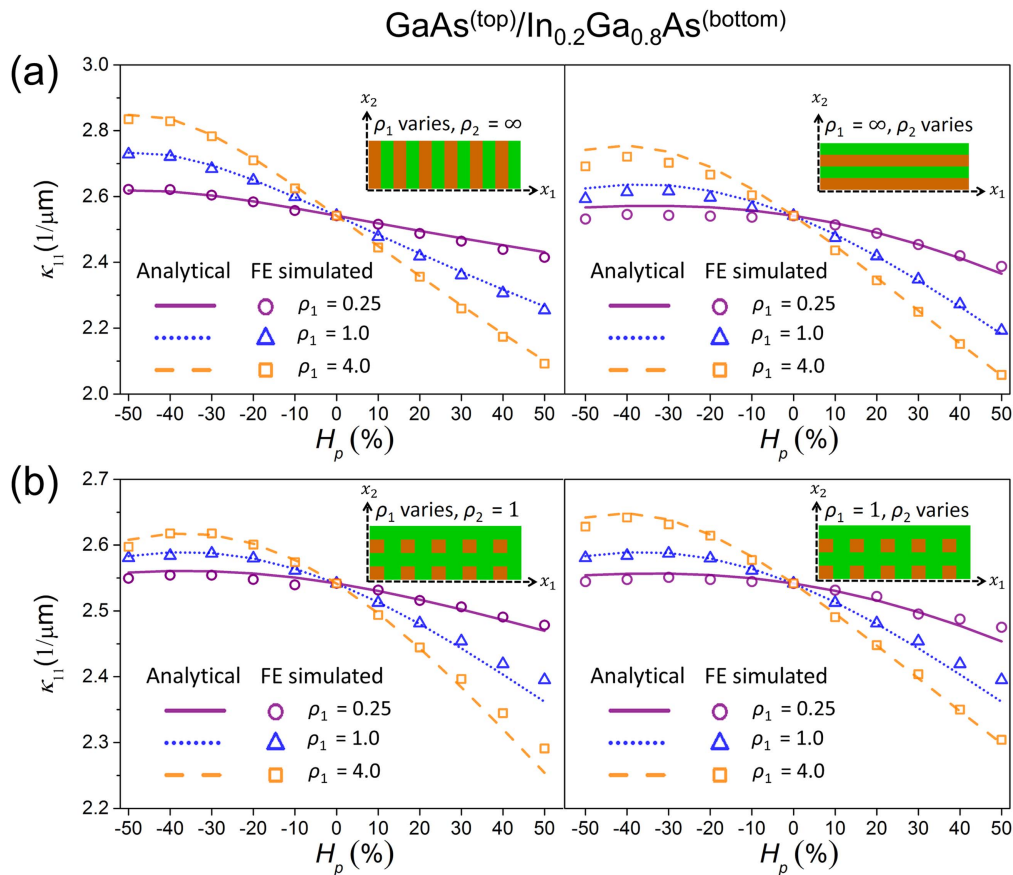


Figure 2. Comparison between the FE simulated (symbols) and model predicted (lines, from equations (6)–(9)) rolling curvature κ_{11} as the pattern thickness H_p and pattern densities (ρ_1 , ρ_2) vary, for the $\text{GaAs}^{(\text{top})}/\text{In}_{0.2}\text{Ga}_{0.8}\text{As}^{(\text{bottom})}$ nanomembrane system with (a) grating and (b) rectangular patterns.

(2) *Category II*: ABAQUS explicit/dynamic package was employed for simulations in this category to investigate the competition between roll-up behaviors along different roll-up directions of strained nanomembranes. Unlike those static simulations in category I, no pre-strain was imposed to influence the roll-up direction of the nanomembrane, corresponding to the situation of isotropic etching release. Simulations in this category focus on strained nanomembranes with grating patterns, examining the role of geometrical anisotropic distribution of grating pattern structures in inducing anisotropic rolling mode and the formation of helical shapes. It is worth noting that the effect of cubic patterns on the roll-up competition was not considered here due to their geometrical isotropy.

3. Results

3.1. Effect of patterning on roll-up curvature for unidirectional rolling

Two nanomembrane systems, i.e., $\text{GaAs}^{(\text{top})}/\text{In}_{0.2}\text{Ga}_{0.8}\text{As}^{(\text{bottom})}$ and $\text{GaN}^{(\text{top})}/\text{AlN}^{(\text{bottom})}$, which are widely used to fabricate self-assembly semiconductor nanostructures with various

geometries [6, 41, 54, 55], are selected as representative systems. The superscripts ‘top’ and ‘bottom’ are used to respectively indicate the materials of the top and bottom layers within the nanomembranes. The corresponding material properties are listed in table 1. The FE simulated evolutions of the roll-up curvature κ_{11} , for controlled unidirectional rolling along the longitude (x_1) direction, as the dimensionless thickness parameter H_p ($=h_p/h_t$) and pattern density parameters (ρ_1 , ρ_2) vary are presented in figures 2 and 3 for $\text{GaAs}^{(\text{top})}/\text{In}_{0.2}\text{Ga}_{0.8}\text{As}^{(\text{bottom})}$ and $\text{GaN}^{(\text{top})}/\text{AlN}^{(\text{bottom})}$ nanomembrane systems respectively. As previously described, negative and positive values of H_p respectively indicate etched and attached patterns. As observed in figures 2 and 3, there is excellent agreement between the FE simulated and analytically predicted (from equations (6)–(9)), which evidences the accuracy and reliability of the analytical model in describing the rolling behaviors of different material systems. It is worth to mention that here FE simulations were used for model validation due to the absence of experimental data on self-rolling of patterned $\text{GaAs}^{(\text{top})}/\text{In}_{0.2}\text{Ga}_{0.8}\text{As}^{(\text{bottom})}$ and $\text{GaN}^{(\text{top})}/\text{AlN}^{(\text{bottom})}$ nanomembranes. Though such rolled-up microtubes using similar material combination have been previously reported, the fabrication involved lots of sophisticated and expensive processes such as the fine tuning of the molecular beam epitaxy, which are far beyond the scope of this research. Nonetheless, it is important to evaluate the model in

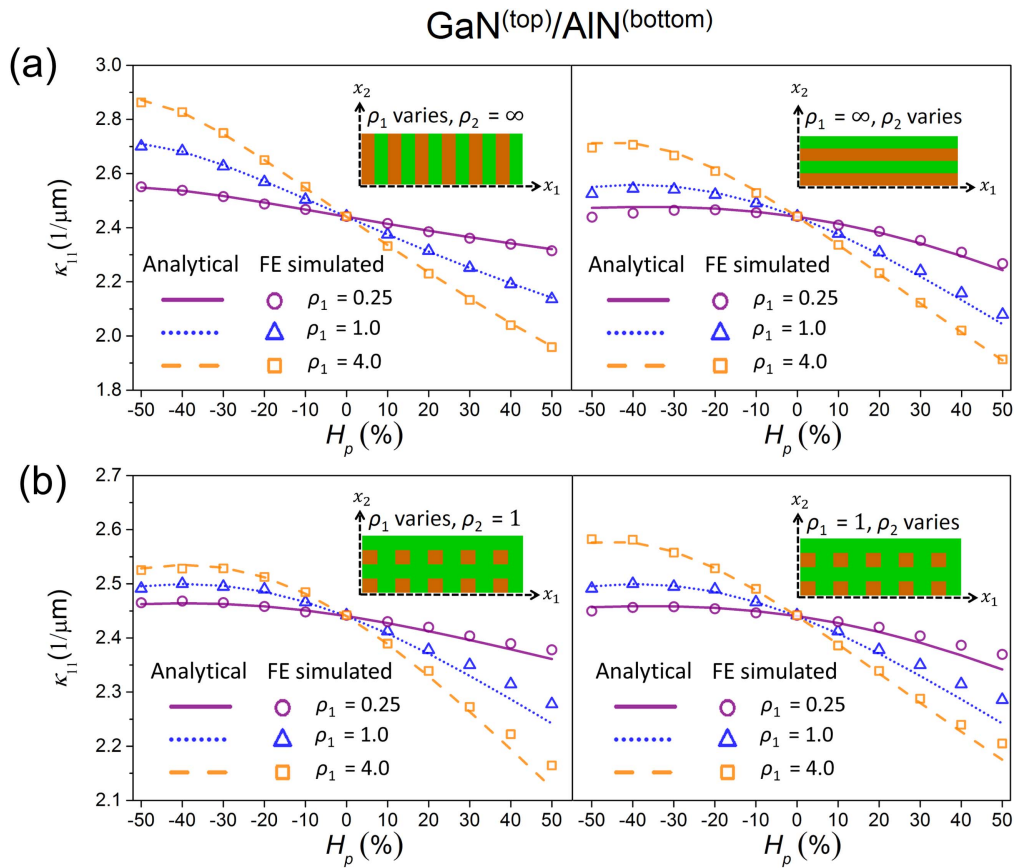


Figure 3. Comparison between the FE simulated (symbols) and predicted (lines, from equations (6)–(9)) rolling curvature κ_{11} as the pattern thickness H_p and pattern densities (ρ_1 , ρ_2) vary, for the GaN^(top)/AlN^(bottom) nanomembrane system with (a) grating and (b) rectangular patterns.

the context of experiments. In this regard, we have included an additional material system, i.e., Ti [25], where experimental data are available (though not complete), for further model validation (details are provided in the supplementary material, available online at stacks.iop.org/NANO/29/345301/mmedia).

As noted in figures 2 and 3, for positive H_p , the increment in pattern density leads to decrease in the longitude rolling curvature κ_{11} , while the opposite dependence of curvature on pattern density is observed for the negative range of H_p . It can also be seen that the influence of both pattern density and thickness on the curvature is less pronounced in the negative range of H_p . Another interesting observation from figures 2, 3 in the negative range of H_p is that the dependence of the curvature κ_{11} on H_p can be non-monotonic, i.e., as H_p decreases from zero, the curvature would increase initially but could start decreasing as H_p gets more negative. This non-monotonic response can be attributed to the competition between strain energy and thickness reduction. The continuous decrease (i.e., more negative) in H_p leads to effective reduction in the overall nanomembrane thickness which facilitates rolling and favors an increase in the curvature, while at the same time it relieves the strain energy, contributing to lower mechanical driving force for the rolling. Therefore, the local maximum the rolling curvature indicates the point where the benefit from thickness reduction is offset by the loss in strain energy density.

Furthermore, it can be observed in figures 2, 3 that the model prediction shows some deviation from the FE simulated result at large pattern thicknesses. Such deviation can be attributed to the approximation with regard to strain gradient in our model. In many experimental fabrications, surface patterns are introduced by the mold imprint [25] or surface etching [56], and consequently the patterned layer is of the same material as the top layer. In such a scenario, at the initial state (before the release of the strained layer), the patterned and top layers are treated as a whole, and zero strain gradient between them is assumed. In the equilibrium state-of-roll-up, the strain gradient between them is determined based on the Von-Karman nonlinear theory [48, 49]. If another type of material is used to introduce patterns, the initial strain gradient depends on their thermal/lattice mismatch strain of different materials of top and pattern layers. The above treatment is a reasonable approximation when the pattern thickness is less or comparable to that of the top layer, but can lead to inaccurate prediction for larger pattern thickness because the gap between patterns can partially relax the built-in mismatch strain in the strained nanomembranes. To remedy the inaccuracy due to such approximation, one way is to introduce different weighting functions that can be fitted to better describe the strain gradient [57] based on the experimental data, where the strain relaxation of patterns can be treated approximately by assuming the patterns are

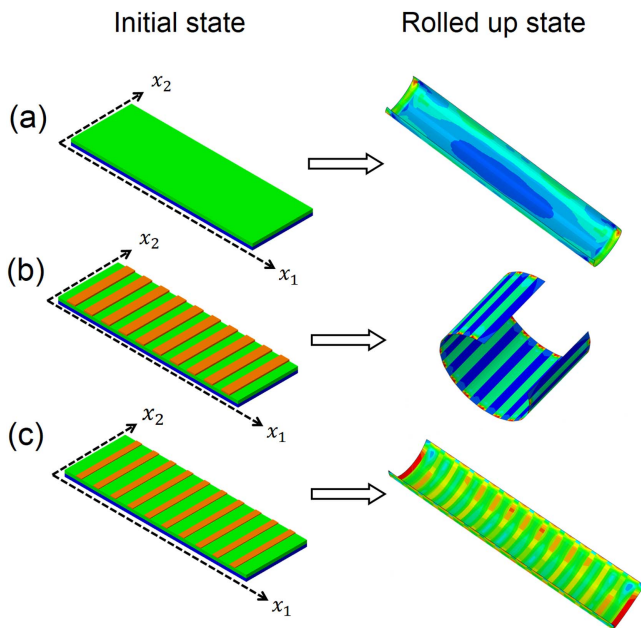


Figure 4. FE simulated results of the rolling behaviors for sample rectangular nanomembranes (a) without and (b) and (c) with grating patterns, with patterns indicated by orange strips, showing the transition of the rolling model from the long-edge (lateral) rolling (a) without or (c) with insufficient grating patterning to short-edge (longitude) rolling (b) with sufficient presence of grating patterns. In this illustrative example, the nanomembrane is assumed to be of GaAs^(top)/In_{0.2}Ga_{0.8}As^(bottom). Sample FE simulation movies illustrating the complete roll-up process available in supplementary material.

completely coherent at their interfaces of the top layer and completely relaxed at the top end of patterns (see supplementary material for details).

3.2. Flexible tuning of rolling direction and roll-up geometry via patterning

Recent experiments on grating-patterned metallic micro-springs reported that the rolling direction of the patterned grating structures in general stays consistently perpendicular to the long side edge of the grating pattern [25], in strong contrast to the rolling behaviors of nanomembranes without surface modifications, which typically exhibit long-edge rolling if not constrained [59]. This indicates the strong ability of grating patterns in regulating the rolling direction of nanomembranes. Nonetheless, so far there exists no dedicated theoretical work to study such regulation. In this regard, here we performed FE simulations, considering a rectangular nanomembrane with grating patterns arranged along the lateral direction (i.e., $\rho_1 > 0$, $\rho_2 = \infty$), as illustrated in figure 4. It was found that the grating patterns, of sufficient thickness (H_p) and density (ρ_1), can transform the originally long-edge (lateral) rolling mode (see figure 4(a)) into short-edge (longitude) rolling mode (see figure 4(b)). More comprehensive FE investigation reveals that the resultant roll-up direction depends on not only the thickness and density of the grating patterns, but also the

aspect (i.e., length/width) ratio R of nanomembranes, as demonstrated in figure 5(a). From figure 5(a), the threshold (H_p , ρ_1) curves corresponding to the lateral-to-longitude rolling mode transition can be identified for nanomembranes of different aspect ratios, and it is interesting to see that those curves effectively coincide into a single curve for large aspect ratios (i.e., $R > 4$). This consolidated curve basically gives the requirement of H_p and ρ_1 that can always ensure nanomembrane rolling perpendicular to the grating pattern.

Another interesting point to note from figure 5(a) is that as the pattern density ρ_1 increases, the H_p required to induce the rolling mode transition quickly decreases and stays nearly a constant value for large ρ_1 values. Given that the grating pattern serves to induce rolling anisotropy (i.e., promoting longitude rolling over lateral rolling), this indicates that the effect of patterning is more prominent at low pattern density. To further understand the above observation, we examine the roll-up curvatures κ_{11} and κ_{22} (predicted from equations (6)–(9)) for the longitude and lateral rolling respectively, and define a parameter $\Lambda = (\kappa_{22} - \kappa_{11})/\kappa_{11}$. The parameter Λ effectively characterizes the magnitude of anisotropy in rolling, and reflects on the different driving forces along the two rolling directions. Figure 5(b) plots Λ as a function of ρ_1 for different H_p . We note that the Λ versus ρ_1 curve gets elevated as H_p increases. For all H_p , Λ is seen to first rapidly increase with the pattern density, and then gradually decay with further increase in the density. The decline in Λ at large ρ_1 suggests that excess pattern density have little influence on rolling anisotropy. Comparing figures 5(a) and (b), we can see that the turning point (in the trend) in the Λ versus ρ_1 curve roughly coincides with the location where the H_p versus ρ_1 curve starts to level out.

The predictive mapping of rolling modes presented in figure 5(a) provides critical guidance for the design of grating structures on nanomembranes, particularly in cases where the regulation of rolling directions is important. Moreover, these insights are also transferable to the design of more complex roll-up geometries. For instance, the predictive design of a helical configuration can be achieved from a grating-patterned rectangular nanomembrane template, as illustrated in figures 6 and 7 and elaborated in details below.

For a grating-patterned rectangular nanomembrane, the rolling direction can be precisely controlled by choosing the appropriate H_p - ρ_1 combination (see figure 5). In particular, for short-edge (longitude) rolling, the grating pattern stays perpendicular to the rolling direction. Now let us consider a strip cut from the nanomembrane, aligned at an angle α to the longitude direction (see figure 6(a)). A series of FE simulations were performed to examine the formation of helical configurations from the rolling of such strips varying thicknesses (h_b , h_p and h_t), pattern density ρ_1 and angle α . It was found that the resultant helical configuration is strongly correlated with rolling behaviors of the host nanomembrane. In particular, the H_p - ρ_1 combination that ensures short-edge (longitude) rolling of the host nanomembranes also prescribes the rolling direction of the strip, leading to helix with axis parallel to the grating pattern, as illustrated

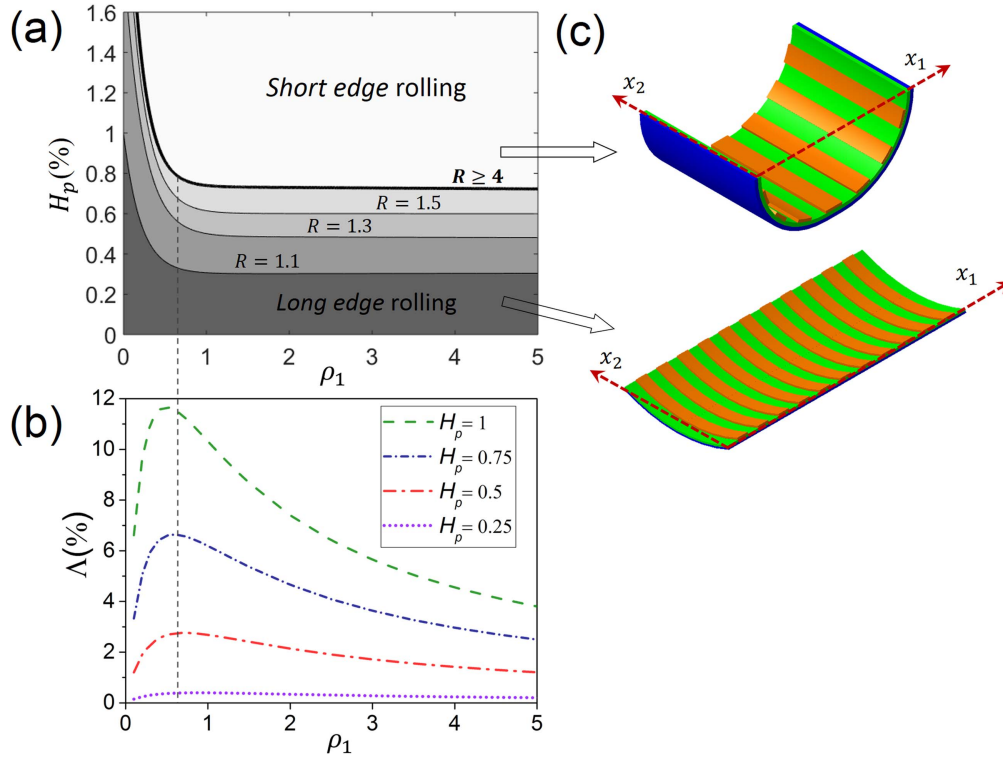


Figure 5. (a) Diagram of preferred rolling modes for the strained, grating-patterned nanomembranes of different aspect ratio R as the H_p and ρ_1 vary, where the regimes above and below the curve (for a particular R) correspond to short-edge (longitude) and long-edge (lateral) rolling respectively. (b) The magnitude of rolling anisotropy between lateral and longitudinal directions are quantitatively measured using $\Lambda = (k_{1a} - k_{1o})/k_{1o}$ as a function of ρ and H_p . (c) shows a schematic illustration of two rolling modes (respectively corresponding to short-edge and long-edge rolling) with grating pattern structures. The patterned and normal strained bilayer are colored in gold, green and blue, respectively. In this illustrative example, the nanomembrane material system is assumed to be $\text{GaAs}^{(\text{top})}/\text{In}_{0.2}\text{Ga}_{0.8}\text{As}^{(\text{bottom})}$.

in figure 7. Meanwhile, interestingly enough, these strips also exhibit nearly identical rolling diameter D with the host nanomembrane (and thus can be predicted by equations (6)–(9)), as demonstrated in figure 6(c). With both the axis and diameter of the helix known, the pitch period (P) of the helix can also be determined:

$$P = \pi D \cdot \tan \alpha, \quad (10)$$

where α denotes the helical angle, being also the angle the strip makes with the longitude direction (see figure 6(a)). On the other hand, within the H_p - ρ_1 domain where the host nanomembrane exhibits long-edge (lateral) rolling, the rolling of the cut strips is much more complex with great variation in the resultant rolling direction and diameter, showing no simple or apparent relation to the rolling of the host nanomembrane, and as a consequence, design of helices with controlled configurations is not feasible (e.g., patterns show random alignment with respect to the helix axis and the helix shows non-straight axis and varying curvature spatially).

The above results demonstrate a new route to achieve predictive design of helices with precise control of their geometry. The fact that we can use a pre-designed, grating-patterned rectangular nanomembrane as the template also

provides interesting design insights towards versatile and flexible fabrication of 3D roll-up nanostructures.

4. Conclusion

Employing both analytical modeling and comprehensive FE simulations, we systematically studied the effect of topological patterning (i.e., grating and rectangular patterns) on the self-rolling behaviors of heteroepitaxial strained nanomembranes. Based on the Von-Karman nonlinear theory and Ritz method, an analytical modeling framework that is capable of predicting the resultant curvature of the patterned nanomembrane has been formulated, with the accuracy and reliability of model prediction validated through FE simulations. Particularly for grating-patterned nanomembranes, it was shown that the rolling direction can be precisely controlled by appropriate selection of the pattern thickness and density. Furthermore, the findings can also directly translate into valuable design insights for more complex roll-up geometries, such as helical structures. As an example, the predictive design of helical structures of desired geometric metrics (i.e., helical angle, pitch period and diameter), resulted from strips cut from a host grating-patterned

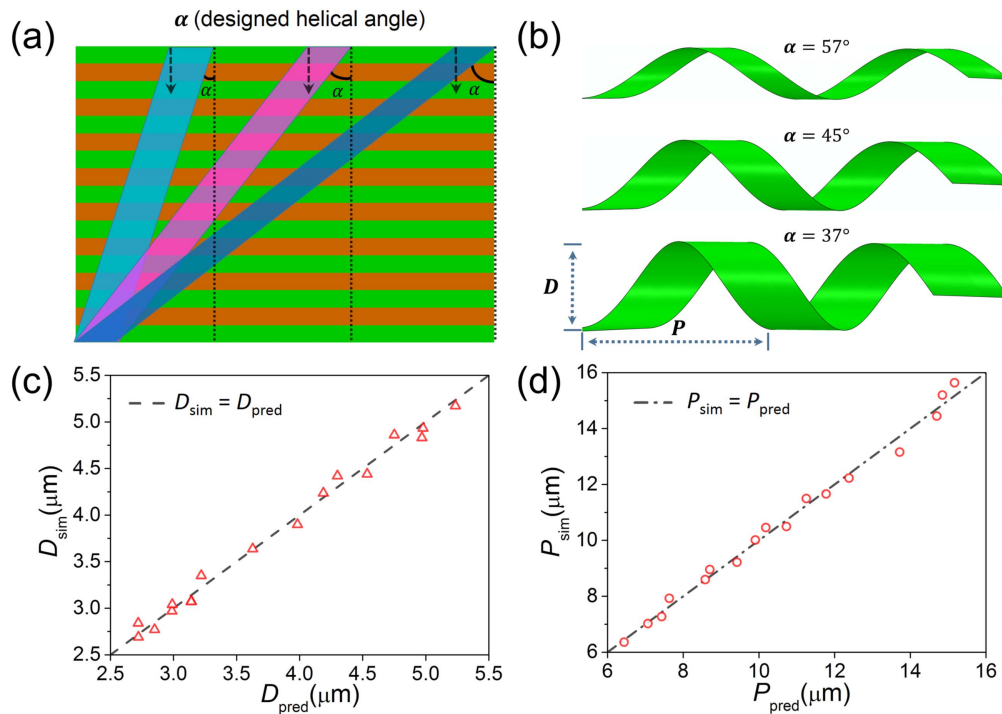


Figure 6. Schematic illustration of (a) strips cut from a grating-patterned host nanomembrane, aligned at different angles α (e.g., $\alpha = 37^\circ$, 45° and 57°) to the direction perpendicular to the grating pattern, which, after roll-up (with the rolling direction indicated by the black dashed arrows in (a)), results in (b) helices with axis parallel to the grating pattern (obtained from FE simulations). (b) FE simulated helical strips with designed helical angles ($\alpha = 37^\circ$, 45° , 57°) with $\rho_1 = 1$ and $H_p = 1$. (c) and (d) plot the designed helix diameter D_{pred} and pitch period P_{pred} (from analytical predictions) against the ones (i.e., denoted as D_{sim} and P_{sim} respectively) obtained from FE simulations, showing excellent agreement. In this illustrative example, the nanomembrane material system is assumed to be $\text{GaAs}^{(\text{top})}/\text{In}_{0.2}\text{Ga}_{0.8}\text{As}^{(\text{bottom})}$. List of data in plots (c) and (d) available in supplementary material.

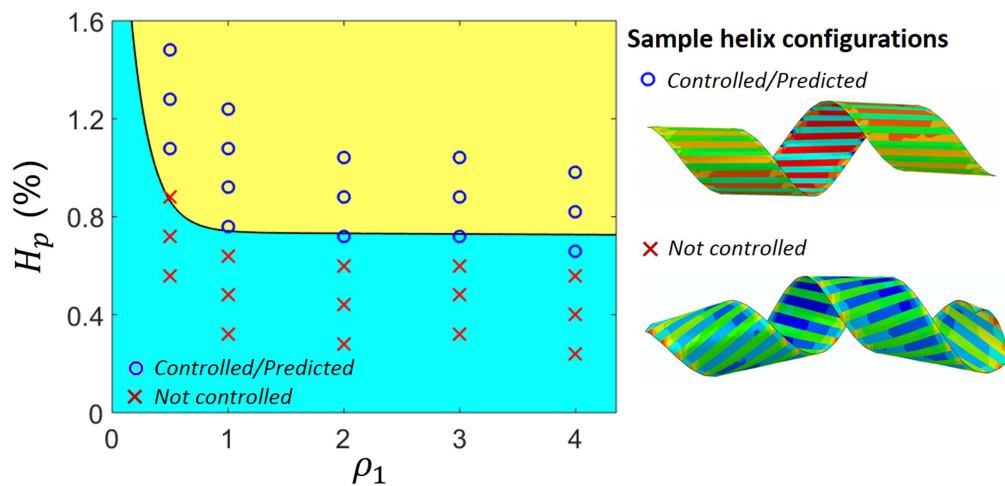


Figure 7. The predictive design diagram of helical configurations formed from the rolling of strips cut from strained patterned nanomembranes as the H_p and ρ_1 vary. The black solid line in the diagram indicates the threshold (H_p , ρ_1) curve corresponding to the lateral-to-longitude rolling mode transition (for $R \geq 4$, also see figure 5(a)). The blue circle and red x-mark symbols indicate whether or not the resultant helical configuration is a controlled one with the helix diameter and pitch period well predicted. In this illustrative example, the nanomembrane material system is assumed to be $\text{GaAs}^{(\text{top})}/\text{In}_{0.2}\text{Ga}_{0.8}\text{As}^{(\text{bottom})}$. List of data available in supplementary material.

nanomembrane was demonstrated. The present study elucidates the pattern induced potential anisotropic self-rolling behaviors and preferred roll-up direction, providing new knowledge and mechanistic guidance towards predictive control and tuning of 3D roll-up nanostructures via topological patterning.

Acknowledgments

We greatly thank the financial support from McGill Engineering Doctoral Award, China Scholarship Council, National Sciences and Engineering Research Council (NSERC) Discovery grant (grant # RGPIN-2017-05187), and NSERC Strategic grant

(grant # STPGP 494012-16). We also acknowledge Super-computer Consortium Laval UQAM McGill and Eastern Quebec for providing computing power.

ORCID iDs

Cheng Chen  <https://orcid.org/0000-0003-3062-9048>

Xinyu Liu  <https://orcid.org/0000-0001-5705-9765>

References

- [1] Janbaz S, Hedayati R and Zadpoor A A 2016 Programming the shape-shifting of flat soft matter: from self-rolling/self-twisting materials to self-folding origami *Mater. Horiz.* **3** 536–47
- [2] Sanchez S 2015 Lab-in-a-tube systems as ultra-compact devices *Lab Chip* **15** 610–3
- [3] Smith E J, Xi W, Makarov D, Monch I, Harazim S, Quinones V A B, Schmidt C K, Mei Y F, Sanchez S and Schmidt O G 2012 Lab-in-a-tube: ultracompact components for on-chip capture and detection of individual micro-/nanoorganisms *Lab Chip* **12** 1917–31
- [4] Schmidt O G and Eberl K 2001 Nanotechnology-thin solid films roll up into nanotubes *Nature* **410** 168–168
- [5] Prinz V Y, Seleznev V A, Gutakovskiy A K, Chehovskiy A V, Preobrazhenskii V V, Putyato M A and Gavrilova T A 2000 Free-standing and overgrown InGaAs/GaAs nanotubes, nanohelices and their arrays *Physica E* **6** 828–31
- [6] Bell D J, Dong L X, Nelson B J, Golling M, Zhang L and Grutzmacher D 2006 Fabrication and characterization of three-dimensional InGaAs/GaAs nanosprings *Nano Lett.* **6** 725–9
- [7] Ma T, Liang H S, Chen G, Poon B, Jiang H Q and Yu H B 2013 Micro-strain sensing using wrinkled stiff thin films on soft substrates as tunable optical grating *Opt. Express* **21** 11994–2001
- [8] Cendula P, Malachias A, Deneke C, Kiravittaya S and Schmidt O G 2014 Experimental realization of coexisting states of rolled-up and wrinkled nanomembranes by strain and etching control *Nanoscale* **6** 14326–35
- [9] Wang J, Zhan T R, Huang G S, Chu P K and Mei Y F 2014 Optical microcavities with tubular geometry: properties and applications *Laser Photonics Rev.* **8** 521–47
- [10] Li S L, Ma L B, Zhen H L, Jorgensen M R, Kiravittaya S and Schmidt O G 2012 Dynamic axial mode tuning in a rolled-up optical microcavity *Appl. Phys. Lett.* **101** 231106
- [11] Tang S W, Fang Y F, Liu Z W, Zhou L and Mei Y F 2016 Tubular optical microcavities of indefinite medium for sensitive liquid refractometers *Lab Chip* **16** 182–7
- [12] Huang S Z *et al* 2017 Tunable pseudocapacitance in 3D TiO₂-delta nanomembranes enabling superior lithium storage performance *ACS Nano* **11** 821–30
- [13] Zhang L *et al* 2014 Hierarchically designed SiO_x/SiO_y bilayer nanomembranes as stable anodes for lithium ion batteries *Adv. Mater.* **26** 4527
- [14] Yan C L, Xi W, Si W P, Deng J W and Schmidt O G 2013 Highly conductive and strain-released hybrid multilayer Ge/Ti nanomembranes with enhanced lithium-ion-storage capability *Adv. Mater.* **25** 539–44
- [15] Wang H and Pumer M 2015 Fabrication of micro/nanoscale motors *Chem. Rev.* **115** 8704–35
- [16] Mei Y F, Solovev A A, Sanchez S and Schmidt O G 2011 Rolled-up nanotech on polymers: from basic perception to self-propelled catalytic microengines *Chem. Soc. Rev.* **40** 2109–19
- [17] Grimm D 2013 Rolled-up nanomembranes as compact 3D architectures for field effect transistors and fluidic sensing applications, *Nano Lett.* **13** 213–8
- [18] Schmidt O G, Deneke C, Kiravittaya S, Songmuang R, Heidemeyer H, Nakamura Y, Zapf-Gottwick R, Muller C and Jin-Phillipp N Y 2002 Self-assembled nanoholes, lateral quantum-dot molecules, and rolled-up nanotubes *IEEE J. Sel. Top. Quantum Electron.* **8** 1025–34
- [19] Bell D J, Dong L, Nelson B J and Golling M 2006 Fabrication and characterization of three-dimensional InGaAs GaAs nanosprings *Nano Lett.* **6** 725–9
- [20] Tian Z, Zhang L, Fang Y F, Xu B, Tang S W, Hu N, An Z H, Zi C and Mei Y F 2017 Deterministic self-rolling of ultrathin nanocrystalline diamond nanomembranes for 3D tubular/helical architecture *Adv. Mater.* **29** 1604572
- [21] Mei Y F, Huang G S, Solovev A A, Urena E B, Moench I, Ding F, Reindl T, Fu R K Y, Chu P K and Schmidt O G 2008 Versatile approach for integrative and functionalized tubes by strain engineering of nanomembranes on polymers *Adv. Mater.* **20** 4085
- [22] Chun I S, Verma V B, Elarde V C, Kim S W, Zuo J M, Coleman J J and Li X 2008 InGaAs/GaAs 3D architecture formation by strain-induced self-rolling with lithographically defined rectangular stripe arrays *J. Cryst. Growth* **310** 2353–8
- [23] Li X L 2008 Strain induced semiconductor nanotubes: from formation process to device applications *J. Phys. D: Appl. Phys.* **41** 193001
- [24] Nastaushev Y V, Prinz V Y and Svitashva S N 2005 A technique for fabricating Au/Ti micro- and nanotubes *Nanotechnology* **16** 908–12
- [25] Huang T, Liu Z Q, Huang G S, Liu R and Mei Y F 2014 Grating-structured metallic microsprings *Nanoscale* **6** 9428–35
- [26] Huang W, Yu X, Froeter P, Xu R M, Ferreira P and Li X L 2012 On-chip inductors with self-rolled-up sinx nanomembrane tubes: a novel design platform for extreme miniaturization *Nano Lett.* **12** 6283–8
- [27] Yu X, Huang W, Li M Y, Comberiate T M, Gong S B, Schutt-Aine J E and Li X L 2015 Ultra-small, high-frequency, and substrate-immune microtube inductors transformed from 2D to 3D *Sci. Rep.* **5** 9661
- [28] Arayanarakool R, Meyer A K, Helbig L, Sanchez S and Schmidt O G 2015 Tailoring three-dimensional architectures by rolled-up nanotechnology for mimicking microvasculatures *Lab Chip* **15** 2981–9
- [29] Hu Y Y and Huang W M 2004 Elastic and elastic-plastic analysis of multilayer thin films: closed-form solutions *J. Appl. Phys.* **96** 4154–60
- [30] Nikishkov G P 2003 Curvature estimation for multilayer hinged structures with initial strains *J. Appl. Phys.* **94** 5333–6
- [31] Tsui Y C and Clyne T W 1997 An analytical model for predicting residual stresses in progressively deposited coatings: I. Planar geometry *Thin Solid Films* **306** 23–33
- [32] Grundmann M 2003 Nanoscroll formation from strained layer heterostructures *Appl. Phys. Lett.* **83** 2444–6
- [33] Zang J, Huang M H and Liu F 2007 Mechanism for nanotube formation from self-bending nanofilms driven by atomic-scale surface-stress imbalance *Phys. Rev. Lett.* **98** 146102
- [34] Chen C, Song P, Meng F, Li X, Liu X and Song J 2017 Quantitative analysis and predictive engineering of selfrolling of nanomembranes under anisotropic mismatch strain *Nanotechnology* **28** 485302

- [35] Cavallo F and Lagally M G 2010 Semiconductors turn soft: inorganic nanomembranes *Soft Matter* **6** 439–55
- [36] Cavallo F, Songmuang R and Schmidt O G 2008 Fabrication and electrical characterization of Si-based rolled-up microtubes *Appl. Phys. Lett.* **93** 143113
- [37] Cavallo F, Songmuang R, Ulrich C and Schmidt O G 2007 Rolling up SiGe on insulator *Appl. Phys. Lett.* **90** 193120
- [38] Kipp T, Welsch H, Strelow C, Heyn C and Heitmann D 2006 Optical modes in semiconductor microtube ring resonators *Phys. Rev. Lett.* **96** 077403
- [39] Deneke C, Muller C, Jin-Phillipp N Y and Schmidt O G 2002 Diameter scalability of rolled-up In(Ga)As/GaAs nanotubes *Semicond. Sci. Technol.* **17** 1278–81
- [40] Jin-Phillipp N Y, Thomas J, Kelsch M, Deneke C, Songmuang R and Schmidt O G 2006 Electron microscopy study on structure of rolled-up semiconductor nanotubes *Appl. Phys. Lett.* **88** 033113
- [41] Li F and Mi Z T 2009 Optically pumped rolled-up InGaAs/GaAs quantum dot microtube lasers *Opt. Express* **17** 19933–9
- [42] Tian Z B, Veerasubramanian V, Bianucci P, Mukherjee S, Mi Z T, Kirk A G and Plant D V 2011 Single rolled-up InGaAs/GaAs quantum dot microtubes integrated with silicon-on-insulator waveguides *Opt. Express* **19** 12164–71
- [43] Tian Z B, Li F, Mi Z T and Plant D V 2010 Controlled transfer of single rolled-up InGaAs-GaAs quantum-dot microtube ring resonators using optical fiber abrupt tapers *IEEE Photonics Technol. Lett.* **22** 311–3
- [44] Freund L B 2000 Substrate curvature due to thin film mismatch strain in the nonlinear deformation range *J. Mech. Phys. Solids* **48** 1159–74
- [45] Vidoli S 2013 Discrete approximations of the Foppl-Von Karman shell model: from coarse to more refined models *Int. J. Solids Struct.* **50** 1241–52
- [46] Dano M L and Hyer M W 1998 Thermally-induced deformation behavior of unsymmetric laminates *Int. J. Solids Struct.* **35** 2101–20
- [47] Hyer M W 1981 Calculations of the room-temperature shapes of unsymmetric laminates *J. Compos. Mater.* **15** 296–310
- [48] Bower A F 2009 *Applied Mechanics of Solids* (Boca Raton, FL: CRC Press)
- [49] Bauchau O A and Craig J I 2009 Kirchhoff plate theory *Structural Analysis* (Berlin: Springer) pp 819–914
- [50] Diaconu C G, Weaver P M and Arrieta A F 2009 Dynamic analysis of Bi-stable composite plates *J. Sound Vib.* **322** 987–1004
- [51] Brunetti M, Vincenti A and Vidoli S 2016 A class of morphing shell structures satisfying clamped boundary conditions *Int. J. Solids Struct.* **82** 47–55
- [52] Barbero E J 2013 *Finite Element Analysis of Composite Materials Using Abaqustm* (London: Taylor and Francis)
- [53] Deger C, Born E, Angerer H, Ambacher O, Stutzmann M, Hornsteiner J, Riha E and Fischerauer G 1998 Sound velocity of $\text{Al}_x\text{Ga}_{1-x}\text{N}$ thin films obtained by surface acoustic-wave measurements *Appl. Phys. Lett.* **72** 2400–2
- [54] Dastjerdi M H T, Djavid M, Arafin S, Liu X, Bianucci P, Mi Z and Poole P J 2013 Optically pumped rolled-up InAs/InGaAsP quantum dash lasers at room temperature *Semicond. Sci. Technol.* **28** 094007
- [55] Mei Y F et al 2009 Fabrication, self-assembly, and properties of ultrathin aln/gan porous crystalline nanomembranes: tubes, spirals, and curved sheets *ACS Nano* **3** 1663–8
- [56] Chun I S, Challa A, Derickson B, Hsia K J and Li X L 2010 Geometry effect on the strain-induced self-rolling of semiconductor membranes *Nano Lett.* **10** 3927–32
- [57] Huang M H, Rugheimer P, Lagally M G and Liu F 2005 Bending of nanoscale ultrathin substrates by growth of strained thin films and islands *Phys. Rev. B* **72** 085450
- [58] Nord J, Albe K, Erhart P and Nordlund K 2003 Modelling of compound semiconductors: analytical bond-order potential for gallium, nitrogen and gallium nitride *J. Phys.: Condens. Matter* **15** 5649–62
- [59] Alben S, Balakrisnan B and Smela E 2011 Edge effects determine the direction of bilayer bending *Nano Lett.* **11** 2280–5